6-kyr record of flood frequency and intensity in the western Mediterranean Alps – Interplay of solar and temperature forcing

Sabatier Pierre[1], Wilhelm Bruno[2], Ficetola Gentile Francesco[3], Moiroux Fanny[1], Poulenard Jérôme[1], Develle Anne-Lise[1], Bichet Adeline[2], Chen Wentao[3], Pignol Cécile[1], Reyss Jean-Louis[3], Gielly Ludovic[3], Bajard Manon[1], Perrette Yves[1], Malet Emmanuel[1], Taberlet Pierre[3], Arnaud Fabien[1]

1 EDYTEM, Université Savoie Mont Blanc, CNRS, 7337 Le Bourget du Lac
2 LTHE, Université Grenoble Alpes, 38000 Grenoble, France
3 LECA, CNRS UMR 5553, Université Joseph Fourier, 38041 Grenoble, France

Abstract:

Abstract

The high-resolution sedimentological and geochemical analysis of a sediment sequence from Lake Savine (Western Mediterranean Alps, France) led to the identification of 220 event layers for the last 6000 years. 200 were triggered by flood events and 20 by underwater mass movements possibly related to earthquakes that occurred in 5 clusters of increase seismicity. Because human activity could influence the flood chronicle, the presence of pastures was reconstructed through ancient DNA, which suggested that the flood chronicle was mainly driven by hydroclimate variability. Weather reanalysis of historical floods allow to identify that mesoscale precipitation events called “East Return” events were the main triggers of floods recorded in Lake Savine. The first part of this palaeoflood record (6–4 kyr BP) was characterized by increases in flood frequency and intensity in phase with Northern Alpine palaeoflood records. By contrast, the second part of the record (i.e., since 4 kyr BP) was phased with Southern Alpine palaeoflood records. These results suggest a palaeohydrological transition at approximately 4 kyr BP, as has been previously described for the Mediterranean region. This may have resulted in a change of flood-prone hydro-meteorological processes, i.e., in the balance between occurrence and intensity of local convective climatic phenomena and their influence on Mediterranean mesoscale precipitation events in this part of the Alps. At a centennial timescale, increases in flood frequency and intensity corresponded to periods of solar minima, affecting climate through atmospheric changes in the Euro-Atlantic sector.

Keywords : Flood frequency and intensity, Lake sediment, Mediterranean Alps, Climate variability, Human activity, Earthquake

1. Introduction

Storms and floods are the most frequent and costly extreme weather events occurring in Europe, representing 69% of the economic losses caused by natural catastrophic disasters between 1980 and 2006 (CEA, 2007). In mountain areas, river flooding is one of the most significant natural hazards, causing widespread damages to infrastructures and human and economic losses (Gaume et al., 2009). Therefore, robust knowledge about their future trends is one of the main scientific challenges for a worldwide sustainable development. This is particularly true in mountainous regions because of their high sensitivity to the ongoing climate warming. For the next century, a modification of the hydrological cycle is expected and may lead to changes in precipitation regime and flood hazard. However, the projections of flood risk are still highly uncertain, mainly because of the complexity in precipitation pattern variations at a regional scale (IPCC, 2013). A recent study, simulated a future a broad-scale summer precipitation reduction in the Alps, but an increase in extreme precipitations over high Alpine elevation areas associated with increased convective rainfalls (Giorgi et al., 2016). However, the spatial and temporal distribution of flood events might be rather heterogeneous in the European Alps (Beniston et al., 2007; Giorgi et al., 2016). But the lack of long-term instrumental data at high-altitude sites do not allow to identify significant trends (Beniston et al., 2007; Westra et al., 2013) and thus, the effects of modern climate change on the frequency and the intensity of extreme precipitation events are regionally difficult. However, robust flood hazard assessment is necessary in the European Alps with the recent demographic and touristic development (Beniston and Stephenson, 2004). Geological data offer opportunities to reconstruct long-term variability of past flood events well beyond the observational record. Lake sediments have been increasingly studied over the last decade to reconstruct long-term flood chronicle (Noren et al., 2002; Bøe et al., 2006; Moreno et al., 2008; Wilhelm et al., 2012a; 2013 ; Vannière et al., 2013; Wirth et al., 2013; Glur et al., 2013; Swierczynski et al., 2013 ; Corella et al., 2014 ; Czymzik et al., 2016) because lake sediments provide a well preserved continuous archive of past flood events.

This study focus on the reconstruction of the past variability in a region, i.e. the French-Italian Alpine border, where the climate is influenced by the Mediterranean climates. Heavy precipitation events triggering floods are related to either local convective phenomena (i.e. summer thunderstorms) or mesoscale convective systems called “East Return” events strongly linked to the cyclonic activity over the Mediterranean area (Garavaglia et al., 2010; Gottardi et al., 2010). This area is affected in the past century by extreme precipitation events with significant damages to houses and infrastructures and several life losses (Ratto et al., 2003; Arnaud-Fassetta and Fort, 2004). The main objective of this study was to identify regional flood patterns using historical and lacustrine (Lake Savine) archives in this region. Here, we present a high-resolution study, based on a multi-proxy method associating sedimentology and geochemistry data from a well-dated long core. Our approach focused on six main challenges: i) identify event layers at the mm scale, ii) distinguish those induced by flood from those induced by mass movements, iii) reconstruct the intensity of past flood events, iv) assess the potential impact of human activities on the recorded flood signal through ancient DNA, v) define the type of precipitation events triggering floods through the study of weather reanalysis and finally vi) discuss the long term variability of paleoflood frequency and intensity in regard to past climatic variations.

2. Study area

2.1 Lake Savine and its catchment

Lake Savine is located in the Haute-Maurienne massif (Fig. 1), approximately 90 km south from Lake Anterne (Giguet-Covex et al., 2011 Fig. 1b) and 105 km north of Lake Allos (Wilhelm et al, 2012a, Fig. 1b). The lake is a rectangular-shape (550 m by 175 m) high-elevation system (2447 m a.s.l., N45°10.500, E6°54.821). Its watershed is formed by a cirque of 3.5 km^2, limited in its south-eastern part by the French-Italian border. The watershed rises up to 3310 m. a.s.l. and is mainly (90%) made up by crystalline rock and Permian gneiss and micaschiste. The upper part of the watershed (North-eastern) is composed by Mesozoic rock with quartzite, cargneule, evaporate (Triassic) and marble and calcareous schist (Jurassic to Cretaceous) (Figure 1c).

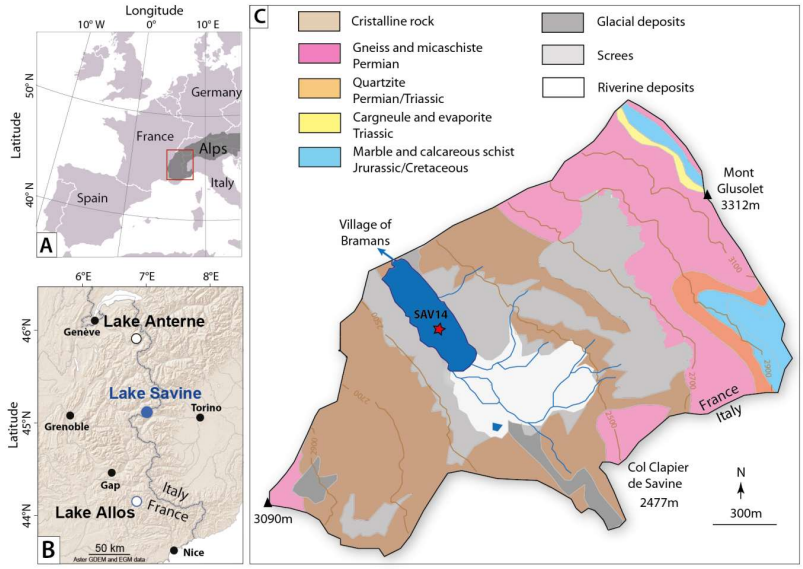

Figure 1: (A) Location of Lake Savine in the western Alps, (B) compared with the locations of the previously studied Lake Anterne (Giguet-Covex et al., 2011) and Lake Allos (Wilhelm et al., 2012a). (C) Geological and geomorphological characteristics of the Savine catchment area.

The main stream of the catchment (Torrent de Savine), drains mainly the south-eastern part of the watershed and has built an alluvial plain (Fig. 1c), suggesting high detrital fluxes. The only evidence that the catchment was glaciated in the past is the moraine in the upper south-western part of watershed. Detrital inputs from these streams are limited to summer and autumn because

the catchment is covered by snow and the lake is frozen from mid-November to mid-June. The Savine stream flows downstream into the Ambin stream and then to the Arc River at the Bramans village 12 km North West from Lake Savine.

2.2 Hydro-climatic setting and historical flood record

The Haute-Maurienne massif is located in the French Alps, bordering with the Italian border (Fig. 1). In this part of the Alps, the climate is influenced by both the Atlantic Ocean and the Mediterranean Sea. As a result, the Haute-Maurienne massif corresponds to a transition zone of Alpine precipitation patterns in the meteorological reanalyses between the Southern and the central French Alps (Durant et al., 2009). Heavy precipitation events are related to either local convective phenomena (i.e. summer thunderstorms) or mesoscale convective systems called "East Return" events occur mainly from late spring to autumn and result from Mediterranean humid air masses flowing northward into the Po Plain and then westward to the Haute-Maurienne Massif (Gottardi et al., 2010; Wilhelm et al., 2016a). Numerous past flood events have been evidenced from studies of local historical documents (ONF-RTM database, http://rtm-onf.ifn.fr/). These historical information show that the Bramans village (located 12 km downstream from Lake Savine) has been affected at least 15 times over the last 150 years by floods of the Ambin torrent and its two main tributaries (Savine and Etache torrents).

3. Material and methods

3.1 Lake coring

A 775-cm-long core was extracted in March 2014 from the frozen surface of Lake Savine, using an Uwitec platform and piston coring devices. The core was retrieved from the deepest part of the lake (7 m depth, N45°10.500, E6°54.821). The SAV14 sediment long sequence (IGSN codes refer to an open international database, www.geosamples.org) is composed of two overlapping core sites, SAV14-01 and SAV14-02, made of three and two sections, respectively. Sections from the second hole were taken following a 1-m shift in depth to ensure a sufficient overlap to provide a continuous record. A short gravity core (SAV14P2) was also taken to provide a well-preserved water–sediment interface sample, which was subsequently correlated to the composite sequence. At the EDYTEM laboratory, the cores were split into two halves. Each half-section was described in detail and pictures were taken with a 20-pixel mm^{-1} resolution. The lithological description of the sequence allowed the identification of different sedimentary facies. A composite sediment sequence (SI1) was built using noticeable layers from the overlapping sections of all cores.

3.2 Sedimentary and geochemistry

The grain-size distribution of the sediment was measured with a 5-mm sampling step on most of the graded deposits along the whole sediment sequence, using a Malvern Mastersizer 2000G laser particle sizer. Ultrasonics were used to dissociate mineral particles and to avoid their flocculation. We then used the median (D50) and the coarsest fractions (D90) to characterize

interbedded deposits (Passega, 1964; Mulder et al., 2001; Wilhelm et al., 2013; 2015). We also recorded the thickness and D90max (i.e. the highest D90 value) of each interbedded deposit.

The core was sampled with a 2-cm interval. These 78 samples (same sample than aDNA) were dried at 60 °C during 4 days to obtain its dry bulk density. Then the Loss Of Ignition LOI of each sample was performed using the protocol of Heiri et al. (2001). The LOI at 550 °C and 950 °C corresponds to the organic and carbonate components of the sediment, respectively.

XRF analysis was performed on the surfaces of the split sediment core with a 1-mm sampling step, using a nondestructive Avaatech core-scanner (EDYTEM) on the whole composite sequence. The split core surface was first covered with 4-µm-thick Ultralene to avoid contamination of the XRF measurement unit and desiccation of the sediment. The geochemical data were obtained at various tube settings: 10 kV and 1.5 mA during 20 s. for Al, Si, S, K, Ca, Ti, Mn, and Fe and, 30 kV and 0.8 mA during 40 s for Cu, Zn, Br, Sr, Rb, Zr, and Pb (Richter et al., 2006). Each individual power spectrum was converted through a deconvolution process into relative components (intensities), expressed in counts per second.

3.3 Ancient DNA (aDNA)

From the sediment core, we sampled 72 slices of 2-cm thickness covering the whole core. To avoid potential contamination, we removed edges of slices that could contain contaminating DNA, in particular due to water circulation along the coring tube. DNA extraction targeted extracellular DNA (Pansu et al., 2015). For each sediment slice, we mixed about 15 g of sediment with 15 ml of saturated phosphate buffer (Na_2HPO_4; 0.12 M; pH ≈ 8) during 15 min. 15 ml of the mixture was then centrifuged (10min at 10000 g). 12 ml of the resulting supernatant were transferred to Amicon ® Ultra-15 10K Centrifugal Filter Devices (Millipore) and centrifuged (20 min at 4000 g) for ultrafiltration and concentration of aDNA. Four hundred µl of the resulting concentrate was kept as starting material for the following extraction steps, using the NucleoSpin® Soil kit (Macherey-Nagel, Düren, Germany), skipping the cell lysis step and following manufacturer's instructions (Taberlet et al. 2012). The DNA extract was eluted in 100 µl of SE buffer. Four extraction controls were performed. DNA extraction and amplification were performed in rooms specifically dedicated to ancient DNA studies in University Grenoble Alpes.

Mammal DNA was amplified with the primer pair P007 (Giguet-Covex et al. 2014), designed to target a short (60- to 84-bp) fragment of the mammal mitochondrial 16S gene. To assign sequence reads to the relevant sample, 8 bp tags (with at least 5 differences between them) were added to the 5' end of primers (Binladen et al. 2007; Valentini et al. 2009). DNA amplifications were carried out in a final volume of 20 µl containing 2 µl of diluted DNA extract. The amplification mixture contained 1.2 U of AmpliTaq Gold® DNA Polymerase (Applied Biosystems), 15 mM Tris-HCl, 50 mM KCl, 2 mM of $MgCl_2$, 0.2 mM of each dNTP, 0.2 µM of each primer and 4.8 µg of bovine serum albumin (BSA, Roche Diagnostic). To limit the amplification of human DNA when amplifying mammal DNA, we also added human-specific, blocking oligonucleotide (MamP007_B_Hum1) After 10 min at 95°C, we performed 45 PCR

cycles: 30 s at 95 °C, 30 s at 50 °C, and 1 min at 72 °C. A final elongation step (7 min at 72 °C) was performed. In addition to extraction controls, we also performed three PCR controls, containing PCR mix but no DNA template, and four PCR positive controls, each containing 0.18 ng of DNA extracted from a marsupial (Dideplhis marsupialis, Didelphidae), absent in Europe. All samples and controls were amplified in 12 replicated PCRs (Ficetola et al., 2015). PCR products were then purified and mixed before sequencing. Sequencing was performed by 2 x 125 bp pair-end sequencing on Illumina HiSeq 2500 platform, which returned 21'192'000 reads.

Commenté [FF1]: HAVE TO CHECK !!!!!!

DNA sequences were filtered using the OBITOOLS software (Boyer et al., 2016), following the protocol described in Pansu et al. (2015). The obtained sequences were assigned to the relevant taxa using ecoTag program that finds highly similar sequence(s) in a suitable database. Here, sequences were compared to global mammal database generated by in silico PCR from EMBL with the ecoPCR program (Ficetola et al. 2010). In the final dataset, we kept only sequences with a match >97% with a mammal genus after taxonomic assignment. As it is difficult to disentangle rare taxonomic units from potential errors at low abundance, we considered a sequence as genuine in a PCR product if was detected with ≥5 reads. In environmental DNA studies, false detections are frequent, i.e. sporadic detections of a species can occur even it is absent. We discarded as contaminants sequences detected frequently in controls (humans and pig). Furthermore, we considered only species confirmed by multiple PCR analyses performed on the same sample. We used site generalized occupancy-detection modelling to jointly estimate the detection probability of species in environmental samples, and the frequency of false detections (Ficetola et al., 2015). Occupancy modelling was performed in a Bayesian framework, following the Lahoz-Monfort et al., (2016), and without zeroing single-detections. To ensure convergence, we ran three different MCMC chains each with 10,000 iterations; the first 5,000 iterations were discarded as burnin. Brooks–Gelman–Rubin diagnostics were approximately for all parameters, indicating convergence (Kéry, 2010). Models were run using the R2jags package in R (Su and Yajima, 2015). The estimates of mean occupancy, detection probability and probability of false detection were then used to calculate the actual probability of species presence in a given sample. This approach allows successfully limiting the presence of false positives in environmental DNA analyses, and the probability of presence can be considered as a measure of the reliability of species presence in a given sample (Ficetola et al., 2016 ; Lahoz-Monfort et al., 2016).

3.4 Chronology

The chronology of the Lake Savine sediment sequence is based on short-lived radionuclide measurements and 12 ^{14}C measurements on terrestrial macro-remains. The short-lived radionuclides in the upper 12 cm of core SAV14P2 were measured using high-efficiency, very low-background, well-type Ge detectors at the Modane Underground Laboratory (LSM) (Reyss et al., 1995). The measurement intervals followed facies boundaries, resulting in a non-regular sampling of approximately 5 mm. 137 Cesium (Cs) were introduced into the environment at the end of the 1950s by atmospheric nuclear weapons tests (peak at AD 1963). The Chernobyl

accident in 1986 also dispersed ^{137}Cs into the northern atmosphere (Appleby et al., 1991). ^{210}Pb excess was calculated as the difference between total ^{210}Pb and ^{226}Ra activities (Golberg 1963). We then used the Constant Flux/Constant Sedimentation (CFCS) model and the decrease in excess ^{210}Pb to calculate the sedimentation rate (Goldberg, 1963). The uncertainty of the sedimentation rate obtained by this method was derived from the standard error of the linear regression of the CFCS model. The ^{14}C measurements were carried out by Accelerator Mass Spectrometer (AMS) at the Laboratoire de Mesure ^{14}C (LMC14) ARTEMIS at the CEA (Atomic Energy Commission) institute at Saclay (Table 1). The calibration curve IntCal13 (Reimer et al., 2013) was used for the ^{14}C age calibration. Then, we used the R-code package "clam" on R software (version 3.0.2 R Development Core Team, 2011) to generate an age model (Blaauw, 2010).

3.5 Weather analysis

Weather analyses are realized using the 20th-century reanalysis (version 2) product by Compo et al (2011), which contains global atmospheric variables since 1871 on a 2◦ grid (hereafter 20CR). The reanalysis is based on the Ensemble Kalman Filter data assimilation system of Whitaker and Hamil (2002) and assimilates observed surface pressure and sea-level pressure every 6 h. All reanalysis data used in the current study relates to the mean of the 56 ensemble members. The atmospheric circulation patterns associated with historical floods recorded in Lake Savine sediments are based on daily mean 500 hPa geopotential height anomalies (Z500) and vertically integrated water vapor transport (hereafter IWT). IWT is computed from the daily fields of specific humidity (q), zonal (u) and meridional (v) wind. The magnitude of daily IWT is calculated in an Eulerian framework as follows:

$$IWT = \left[\left(\int_{1000}^{300} qu\frac{dp}{g}\right)^2 + \left(\int_{1000}^{300} qv\frac{dp}{g}\right)^2\right]^{\frac{1}{2}}$$

where g is the acceleration due to gravity. The vertical integration is limited to the 1000 to 300 hPa pressure interval because specific humidity in the 20CR data is negligible above 300 hPa.

4. Results

4.1 Core description and lithology

The upper 7 meters of sediment consists of dark to very dark olive silt composed by 5+/-1.3 of LOI550 (organic matter, OM) and 7.5+/-1% of LOI950 (CaCO3) representing the background hemi-pelagic sedimentation (named BS for background sedimentation, Fig. 2). Below 7 meters the sediment consists of homogenous light grey clay to silt with 2+/-0.1% and 6.8+/-0.1% of LOI950 (SI1). As no plant marcro-remains requested for (radiocarbon) dating, was found deeper than 5.7 m, this study focus on the upper 5.7 m of the Savine sedimentary record. The upper 5.7 m of fine grained deposits are interrupted by 220 graded layers which are interpreted to represent short-term depositional events, i.e. turbidite (Sturm and Matter, 1978 ; Arnaud et al., 2002).

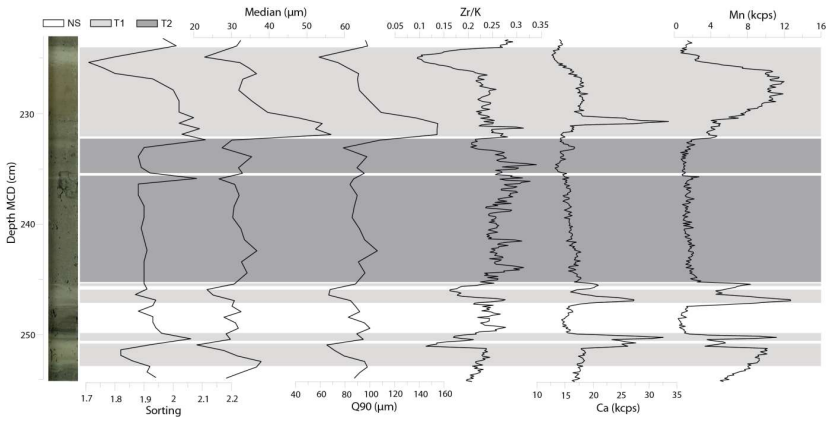

Figure 2: photography, grain size and geochemical data of the three sedimentary facies of SAV14. (BS: background sedimentation in white, T1 in light grey and T2 dark grey).

The 220 event layers are divided in two types of deposits based on their grain size and geochemical patterns. Type-1 (T1) deposits are light-grey graded bed with no evidence of erosive base (Fig. 2). These 200 T1 deposits are characterized by a silty-to-sandy base, a central part with a regular decrease of both D50 and D90 and a very light-grey clayey capping layer (Fig.2). The bottom of these T1 deposit presents relatively high sorting value (most of time > 2, Fig. 2). The geochemical pattern of these T1 deposits is characterized by relatively high Zr intensities at the base of layers and high K intensities in the clay cap, suggesting Zr enrichment in the coarser sediment fraction and K enrichment in the finest fraction. The Zr/K is thus supposed to be a high-resolution proxy of grain-size (Wilhelm et al., 2013). However, the relation between Zr/K and grain size parameters is not well constrain and thus this geochemical cannot be used as high-resolution grain-size proxy, but is used to identify T1 deposit. Ca intensities in these deposits show high values (Fig. 2), simultaneously to high values of LOI950, suggesting high carbonate contents. This Ca increase probably reflects detrital calcareous inputs coming from the eastern part of the watershed, through torrential activity. Mn intensities also show high values in T1 deposits (Fig. 2) that probably reflects the oxygenation state of the water column (Calvert and Pedersen, 1993; Elbaz-Poulichet et al., 2014). Finally, the thickness of the T1 deposits varies between 2 to 170mm (Fig. 3).

The Type-2 (T2, Fig. 2) deposits are made of a main homogeneous, olive to grey, silty part topped by a light grey mm-thick clay cap. The grain size parameters (median, D90) does not show any significant variations except in the clay cap where lower values of median and D90 are observed (Fig.2). The sorting of T2 deposits always presents weak values (around 1.9) except in the upper samples of each deposit due to a mix between the silts of the main part and the clay cap because the sample size. Geochemical data present a constant and relatively high Zr/K ratio, except in the clay cap, and low values of Ca and Mn intensities (Fig. 2).

Finally a remarkable 22 cm reversal sequence is observed between 196 and 218 cm of the mastercore overlapped by a 17cm turbidite (SI3) probably resulting from a large subaquatic landslide.

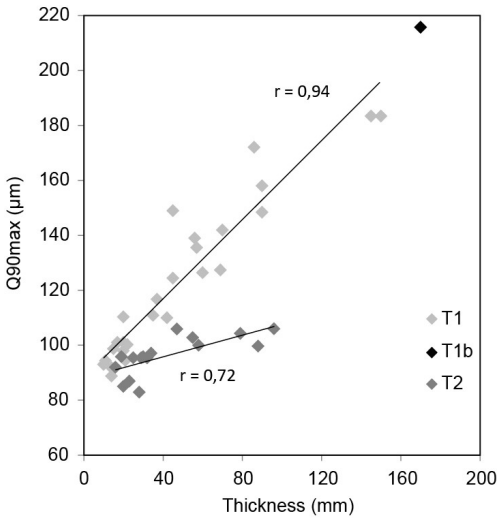

Figure 3: D90max-deposit thickness diagram for T1 and T2 deposits. T1b corresponds to the mass-movement-induced deposit above the reversal sequence, see SI3.

A deposit thickness versus D90max diagram of all T1 (n=26) and T2 (n=16) deposit thicker than 1 cm highlights two distinct patterns (Fig. 3). The T1 deposit named T1b in the Figure 3 corresponds to the thicker layer (170mm) and is not taken into account in this comparison because it is localized at the top of the reversal sequence (SI3). A significant positive linear relationship between bed thickness and D90max ($r=0.94$, $p< 10^{-12}$) is observed for the T1 deposits (Fig. 3), suggesting that higher was the volume of sediments transported and deposited, higher was the grain size of the mobilized sediments. For the T2 deposits, a distinct pattern is observed with a high variability of deposit thickness without high variations in D90max. This suggests that the volumes of sediments transported and deposited to form T2 deposits are poorly related to the grain size.

4.2 Ancient DNA

We detected the DNA of four taxa of mammals: *Bos* (cattle), *Canis* (dog), *Felis* (cat) and *Ovis* (sheep). However, only cattle and sheep were detected in more than one sample by multiple PCR replicates, therefore we will focus the analyses on these two species, while we assumed the presence of dog and cat to be sporadic.
Sporadic detection of cattle DNA occurred in old sediments (below 332 cm). However, in these cases sheep DNA was only detected in one of the 12 PCR replicates performed on each

sediment slice, as a consequence the reliability of these sheep detections was low. Conversely, cattle and sheep DNA was consistently detected between 289 and 307 cm in multiple PCR replicates per sample, indicating high reliability of the presence of these species in this short period (Fig. 6e-f).

4.3 Chronology

4.3.1 Short-lived radionuclides

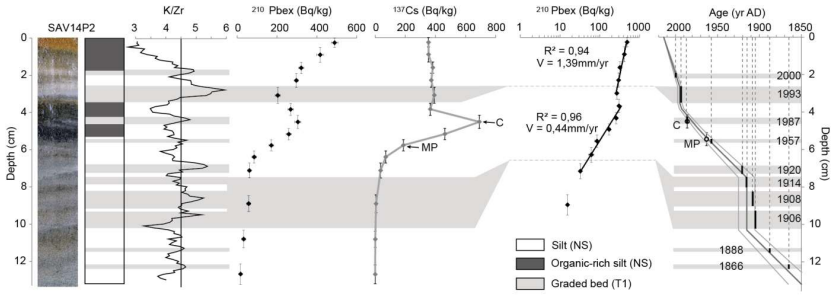

Figure 4: Chronology (with 1σ uncertainties) of the uppermost part of core SAV14P2 based on (a) the short-lived radionuclides (^{210}Pbex and ^{137}Cs) and (b) the application of a CFCS model to the event-free sedimentary profile of ^{210}Pbex. Uncertainties of ^{210}Pbex and ^{137}Cs activities are included in dots Dates on the right-hand side correspond to historical flood dates, possibly associated to the most recent T1 deposits.

The excess ^{210}Pb profile showed a regular decrease punctuated by drops in ^{210}Pbex on the profile (Figure 4). Following (Arnaud et al., 2002), these low values of ^{210}Pbex corresponding to T1 deposits and were excluded in order to construct a event-free sedimentary record because they are considered instantaneous deposits. ^{210}Pbex activities plotted on a logarithmic scale revealed two linear trends providing two mean accumulation rates with of 1.39 +/- 0.2 mm.yr^{-1} above 4.5 cm and 0.44 +/- 0.04 mm.yr^{-1} below this depth. Ages were then calculated using the CFCS model applied to the original sediment sequence to provide a continuous age-depth relationship. In addition, the profiles of ^{137}Cs profile present one main peak at 4.5 cm with a very high activity 692 +/- 6 Bq.kg^{-1}. In this area the ^{137}Cs activity due to maximum nuclear weapons tests in the Northern Hemisphere in AD 1963 present a value between 40 and 300 Bq.kg^{-1} (Wilhelm et al., 2012b; Jenny et al., 2013; Alric et al., 2013; Sabatier et al., 2014; Bajard et al., 2015; Guédron et al., 2015). This very high activity clearly corresponds to the Chernobyl accident in AD 1986 and the localization of the study site at the border between France and Italy strengthened this interpretation, because Italy present larger ^{137}Cs fallout due to this accident. The AD 1963 peak is thus below this main peak and probably around 5.8cm when ^{137}Cs activity reach the range of value cited above. These two artificial markers are in good agreement with the CFCS age model over the last century (Figure 4).

4.3.2 Radiocarbon dating

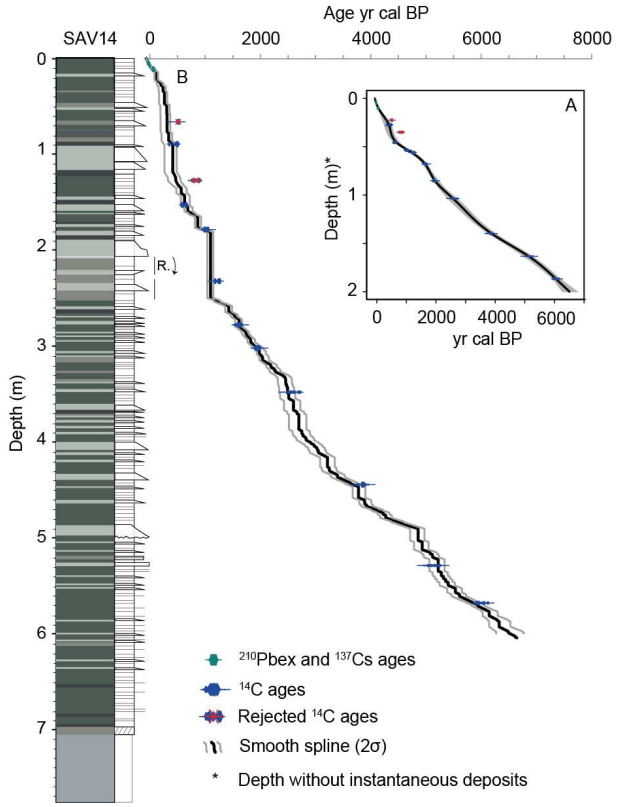

Figure 5: (A) Age-depth model of the event-free sediment record based on radiocarbon and short-lived radionuclides derived ages. (B) Age-depth model for the whole SAV14 sediment sequence. R. indicates the reversal sequence see SI3.

A number of 12 samples are dated for ^{14}C ages (table 1). Two radiocarbon ages were excluded because they appear too old, resulting in age inversions if included (Figure 5). The 220 deposits interpreted as instantaneous events and the reversal sequence (SI3, noted R. in figure 5), representing 391cm of instantaneous deposits, were removed. The remaining 200cm (Fig. 5A) are used to build an event-free sedimentary record (Bøe et al., 2006; Wilhelm et al., 2012a, 2013, Fig. 5A). We then calculated an age-depth relationship via a smooth spline interpolation using the R-code package "Clam" version 2.2 (Blaauw, 2010). The age-depth model is used to date all instantaneous deposits. The vertical bars represent the age of each flood thicker than 5 mm, and uncertainties (2σ) result from the ^{14}C ages (Fig. 5B). The first 565 cm of the Savine sediment sequence cover the last 5.8 kyr BP, The mean sedimentation estimated from the event-

free sediment record varies between 0.2 to 0.4 mm.yr^{-1} with a short term increase to 0.6 mm.yr^{-1} between 1.95 to 1.65 kyr BP, to 1.4 between 0.35 and 0.55 kyr BP and during the last 40 years (Fig. 6D).

5. Discussion

5.1 Instantaneous deposits

5.1.1 Flood-induced deposits

Normally graded beds as T1 deposits are common features of lake sediments, where they are associated with turbidity currents triggered by gravity reworking or flood events (Sturm and Matter, 1978; Arnaud et al., 2002; Gilbert et al., 2006). In the thickness–D90max diagram, T1 deposits are grouped in a distinct cluster, suggesting that they result from the same trigger (Figure 3). In addition, the increase of both transported/deposited sediment volumes and grain size characterizing T1 deposits (Fig. 3) is consistent with sedimentary processes regulated by water currents (e.g. Wilhelm et al., 2013; 2015). Higher discharge rates would lead to a greater sediment supply and coarser materials to the lake system. The 200 T1 deposits are also characterized by Mn increases suggesting that changes in redox conditions occurred in the lake system. In oxic waters, Mn occurs as Mn(IV) in the form of Mn diffuses downwards where it can precipitate as MnCO3 or Mn–Ca carbonates (Calvert and Pedersen, 1993; Pedersen and Price, 1982), and upwards where it can precipitate as Mn oxides at the oxic/anoxic boundary (Elbaz-Poulichet et al., 2014). This process leads to Mn enrichments in surface sediments overlain by oxic bottom waters (Calvert and Pedersen, 1993). When the bottom waters are anoxic, Mn(II) diffuses to the water column and Mn is depleted in the sediments. The presence of Mn in the graded layers associated to Ca (Figure 2) suggests that hyperpycnal turbidity currents carry oxygen to the deepest parts of the basin (Wilhelm et al. 2016a) and produce rapid precipitation of Mn–Ca carbonates in the sediment (Calvert and Pedersen, 1993). In addition, we compared the historical flood calendar from the Ambin torrent and its two main tributaries to the instantaneous deposits recovered in the lake sediment for the last 150 years. Ten historical flood events occurred in AD 2000, 1993, 1987, 1957, 1920, 1914, 1908, 1906, 1888 and 1866 and correspond well to the age of T1 deposits identified through the Zr/K ratio over the first 13cm depth (Figure 4). All these arguments strongly support that T1 deposits are induced by floods.

The good relationship between Q90max and thickness of T1 deposits allowed us to use flood-layer thickness as a high-resolution proxy for stream velocity during flood events (Molinaroli et al., 2009; Parris et al., 2010) and therefore as a proxy for flood intensity (Wilhelm et al., 2013; 2015).

5.1.2 Mass-movement-induced deposits

The thickness-D90max diagram revealed thatT2 deposits result from distinct processes than T1 deposits. This diagram also suggested that the volume of transported/deposited sediments can largely vary without significant variations of grain size. The constant mean grain-size and the stable values of sorting are typical of mass-flow deposits (Mulder and Cochonat, 1996). T2 deposits show only a thin fining-upward sequence followed by a thick homogenous interval with no inverse grading at the base. In addition, these homogeneous layers do not present any increase of Mn content (Figure 2). This suggests that the turbidity currents triggering T2 deposits do not allow to carry oxygen in the deepest part of the basin and are thus probably related to subaquatic mass movements, reworking the material of the lake shores (Wilhelm et al., 2016b). A similar type of mass-movement-induced facies has been previously described and called ‘‘homogenites’’ or ‘‘seiche deposits’’ in lacustrine environments (Chapron et al. 1999; Beck 2009, Petersen et al., 2014). According to these authors, a mass movement would induce a mass transport or slumps, which in turn form hyperpycnal (turbidity) currents with bed-load and suspended-load (Beck 2009). The bed-load sediment would produce the coarse base of the layers, whereas the suspended-load sediment would be homogenized by an oscillatory movement of the whole lake-water mass, i.e. a ‘seiche’ effect. Finally the remarkable reversal sequence topped by the T1b deposit (SI3) is also related to a mass movement.

5.2 Earthquake record

Earthquake shaking appeared to be one of the most common factors that triggers mass movements in high-elevation alpine lakes (Wilhelm et al., 2016b). To test the earthquake trigger of the T2 deposits, ages of the most recent T2 deposits can be compared to dates of regional historical earthquakes well documented over the last centuries (Lambert and Levret-Albaret, 1996; Scotti et al., 2004).

Over this period, one T2 deposit is recorded in AD 1755 (between 1820-1710 yr AD at 2σ of uncertainties). At that time three historical earthquakes occurred: in AD 1808 (Valle del Pellice, 8 MSK), AD 1785 (Valle del Susa, 7.5 MSK) and AD 1767 (Valle di Lanzo, 8 MSK) (Boschi et al., 2000). To discriminate which earthquake is responsible of this deposit, epicentral MSK intensity of all historical earthquakes were plotted against the distance of each earthquake to the lake (SI4). Historical earthquakes, supposed to have triggered T2 deposits, are expected to have generated the strongest ground motions in the lake area. This diagram clearly highlights that the 1785 earthquake is both the strongest and the closest to the lake (SI4). The calculation of the Earthquake Sensitivity Threshold Index ESTI defined by Wilhelm et al., (2016b) is estimated to 0.15± 0.01 for Lake Savine and is in the observed trend for other Alpine lakes.

From the 5600 years of sedimentary record a total of 20 supposed earthquakes-induced deposits were identified through T2 deposits and are spread in 5 clusters of seismicity over time (Figure 6A) with periods of an increased occurrence of earthquakes around 5220, 4250-3800, 3100-2000, 1450-1050 and 350-150 yrs cal BP. Interestingly, most of T2 layers (10 of 20) present no background sediment between deposits that could be interpreted as the record of both earthquake and their respective aftershock. The earthquake-induced deposit recorded around 5220 yr cal BP (5060-5335 at 2σ) could correspond to an event record at a regional scale in three other lakes located more than 115km away in the Northern French Alps (lakes Le Bourget,

Paladru and Blanc Huez; Chapron et al., 2016). This suggests the occurrence of a high magnitude earthquake.
It should be pointed out that the ESTI value was found to be highly dependent on the sedimentation rate (Wilhelm et al., 2016b). Because of the high variations in the Savine sedimentation rate (Fig. 5), the Lake Savine sensitivity to record earthquake may have changed over time. But, in spite of the last cluster, these periods of relatively high earthquake occurrences correspond mainly to low sedimentation rate and could be thus associated to a clusters of seismicity in this region, as suggested by Ratzov et al. (2015) in the west Algeria area.

5.3 Human activity

The climatic information from Savine flood record can be considered relevant over the last 5600 yrs cal BP (Figure 6B, C) if no major changes occurred in erosion processes. Erosion processes in the Savine catchment may be affected by geomorphological modifications and/or by land-use changes link to human activities (i.e. grazing).
Even if the modern watershed is not glaciated, during past clod period such as the Little Ice Age (LIA) substantial activity of small glaciers can modify the sediment availability (Koppes and Hallet, 2002; Hodder et al., 2007). However, the conservation throughout the considered period of the grain-size versus thickness correlation suggests that the relationship between the intensity of flood events and the volume of transported material remained constant and not affected by glacial cover (Fig. 3, Wilhelm et al., 2012b, 2013; Fouinat et al., accepted). Moreover no glacial moraine is present in the watershed. Finally, the main transported sediment stream is oriented toward the South, thus limiting the effect of permafrost activity during Holocene cold periods.

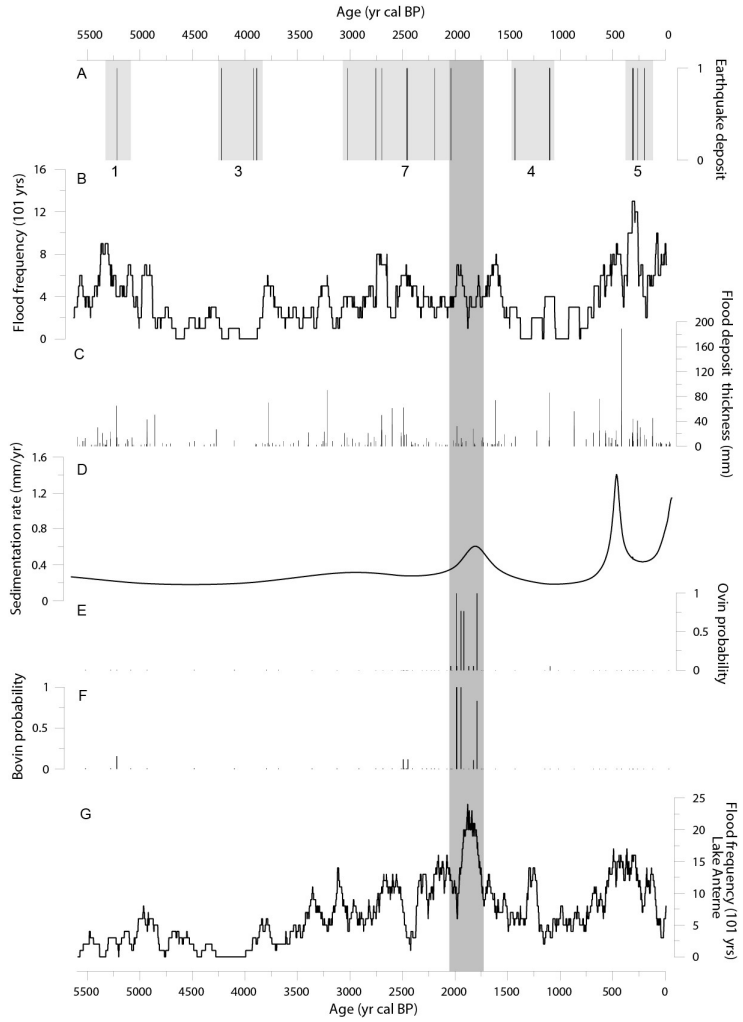

Figure 6: Comparison of (A) reconstructed earthquake events (light grey bands represent period of high seismic activity with the associated number of earthquake during these periods), (B) flood frequency (101 yrs running average) and (C) flood intensity (thickness of flood deposits), (D) average sedimentation rate without instantaneous deposits (earthquake and flood > 5mm), (E) Ovin and (F) Bovin presence probability on the watershed, all these data are produced from Savine record. (G) Anterne flood frequency (101 yr running average) from Giguet-Covex et al., (2011), the vertical grey band is the period of high human activity both in Savine and Anterne lake sedimentary record.

Lake sediment aDNA is used in this study to trace relationships between past landscape changes in relation to past agro-pastoralism activities (mammal DNA) and erosion. At this altitude, the presence of aDNA from domestic animals may be considered as a proxy of that mainly corresponds at this altitude to changes in grazing intensity (Etienne et al., 2013; Giguet-Covex et al., 2014 ; Wilhelm et al., 2016a). An increase of grazing pressure may make soils more vulnerable to erosion during heavy rainfalls leading to an increasing erosion rate and, thereby, an increased sensitivity of the catchment-lake system to record floods (Giguet-Covex et al., 2012). Mammal aDNA show the presence of ovin and bovin in the Savine catchment only during the restricted period between 2050 and 1750 yrs cal BP, known as the Roman Period (Figure 6E, F). This Roman Period with high pastoralism activity is synchronous in Anterne lake record with presence of both ovin and bovin herds (Giguet-Covex et al., 2014). Such increase in human activity during the Roman Period was already recognized at the scale of the Northern French Alps at low (e.g. Lake Moras, Doyen et al. (2013), Lake Paladru, Simonneau et al. (2013), medium (Lake La Thuile, Bajard et al., 2016) and high altitude (Lake Anterne, Giguet-Covex et al., 2011) sites. This resulted in a drastic rise in erosion fluxes in all these lakes. In Lake Anterne, Giguet-Covex et al., (2011) showed that this drastic change of landuse also resulted in the highest flood frequency recorded over the Holocene (Figure 6G) and in a distinct pattern in grain size versus deposit thickness of flood layers.

In Lake Savine, during the first part of the period marked by high grazing pressure, the flood frequency is relatively high, but lesser than during periods without grazing pressure, e.g. 5.3, 2.6, 1.7 or 0.3 kyrs BP (Figure 6B). Moreover, there is no changes in the grainsize versus deposit thickness pattern during this period (Figure 3) as observed in Lake Anterne due to grazing-induced changes in erosion processes (Giguet-Covex et al., 2011). Hence, it seems that that the presence of ovin and bovin in the watershed had a minor influence on erosion processes and, thereby, on the reconstructed flood chronicle.

The unique influence of pastoralism on Savine catchment is the observed increase of mean sedimentation rate (without flood layers) during this period, suggesting that herds and sediment source transported during flood event are not at the same location on the watershed. The sediment source during flood events is located in the South-eastern part of the lake with the presence and probably the reactivation of alluvial fan in this part of the catchment (Figure 1). While the pastoralism activities are probably more restricted to the flat and grassed part i.e. close to the Eastern part of the lake shore and on the delta, as suggested by modern observations (Giguet-Covex and Walsh, pers. com.).

5.4 Paleoflood activity

The comparison between ages of the recent flood deposits and dates of historical floods showed a good agreement (Fig. 4). Moreover, the absence of evidence about significant changes in erosion processes, due to changes in geomorphological and/or human activities, in the Savine catchment makes us confident to interpret the Savine flood record from a paleoclimate point of view.

5.4.1 Historical floods

Weather reanalysis of the last 8 historical floods recorded in the Savine sediment sequence have been performed to better understand the atmospheric circulation patterns (e.g. Rimbu et al., 2016). Two main groups of flood-related synoptic configurations have been identified from 500 hPa geopotential height and Integrated Water Transport (IWT) analysis (Fig. 7). The first group, name Group-1, corresponding to 6 out of 8 flood events (15/10/2000, 24/09/1993, 12/06/1957, 24/09/1920, 23/07/1914 and 20/06/1908) and the second, named Group-2 with 2 out of 8 of events (24/08/1987 and 03/07/1906). All these floods occurred between mid-June to mid-October. The 500 hPa geopotential height for Group-1 events shows a low pressure anomaly over the Bay of Biscay at D-2 that moves south-eastern wards over the north Mediterranean area at D-1 and D. This pattern triggers a cyclonic circulation around the low pressure anomaly that is expected to pick-up moisture from the Mediterranean Sea and favor rainfall into the Po Plain. This pattern resembles at the weather pattern "WP6" identified from 1000 hPa geopotential height in Garavaglia et al. (2010). The IWT for Group-1 events shows an increase of moisture in the north-western Mediterranean area at D-2, followed by a moisture maxima and a marked advection northward into the Po Plain at D-1 and D. This atmospheric circulation pattern is typical of the late spring to autumn, mesoscale events called “East-return” events circulation associated with heavy rainfalls along the Italian border (Garavaglia et al., 2010; Gottardi et al., 2010; Lionello et al., 2012). The warm humid air masses are thus vigorously uplifted with the steep Alps orography causing an abrupt cooling of the air masses and intense precipitations, typical of the in the Mediterranean climate. Two of the recorded Group-1 events (June 1957 and October 2000) are regional catastrophic floods having affected many areas in the French and Italian Alps (Ratto et al., 2003; Arnaud-Fassetta and Fort, 2004). It clearly appears that Group-1 event is the dominant mechanism to produce historical floods recorded in Lake Savine sediment sequence. The geopotential height for Group-2 events show a generalized high pressure anomaly over Europe, with two main centers located over north-eastern Eurasia and northern Atlantic Ocean. This pattern triggers an anticyclonic circulation over the area of interest, which hampers rainfall in this area. It resembles the weather pattern "WP8" identified from 1000 hPa geopotential height in Garavaglia et al. (2010) that is associated with a lack of rain over Europe. The IWT for Group-2 events is null around the study site during D-2 and D-1, while low values of IWT are observed in a much more restricted continental area at D. The weak activity of the atmospheric circulation at the synoptic scale and the event occurrence at the summer season suggest that these two floods events result from localized phenomena like thunderstorms.

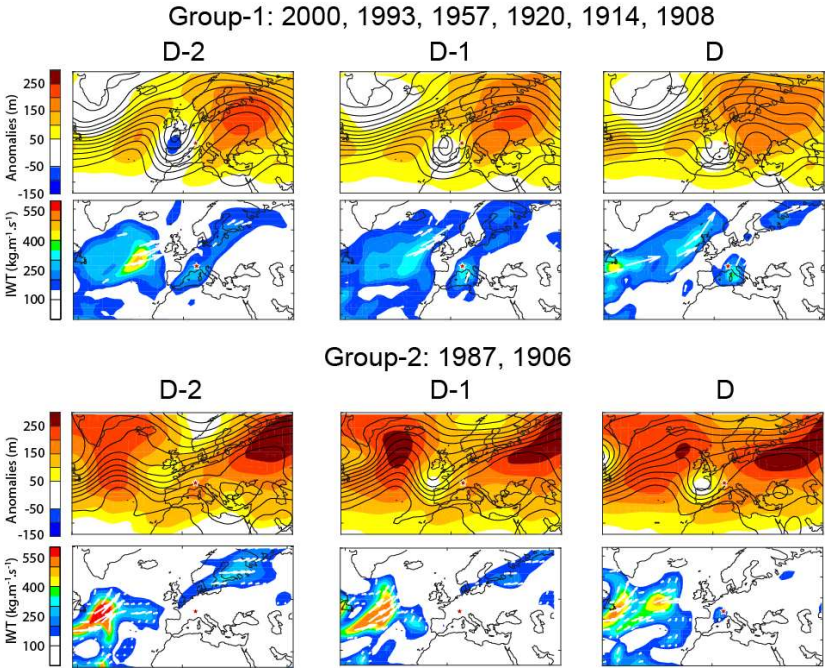

Figure 7: Composite map of both 500 hPa geopotential height (contour) and anomalies (shaded) and of IWT at the day of the historical flood (D) and the two days before (D-1 and D-2). Analyzed events are those recorded in Savine lake sediment. Red star is the Savine lake location.

5.4.2. Savine flood chronicle and climate forcing

Because floods recorded during the last centuries were mainly triggered by mesoscale precipitation events, we assume, in a first step, that the Savine palaeoflood record mostly represents the variability of such events over the whole studied period (figure 8A, B). At multi-centennial timescale the Savine record shows five periods of high flood frequency between 5.6-4.85, 3.9-2.35, 2-1.5, 1.15-1.05 and 0.65-0.05 kyr BP. These increases in flood frequency are associated to the occurrence of the most intense floods (Figure 8B). Only one extreme flood occurs during a period of low flood frequency around 900 years BP. Over the last millennium, this corresponds to a high flood frequency and intensity during the long and cool Little Ice Age (LIA, AD 1300 – 1900) and a lower flood frequency and intensity during the Medieval Climate Anomaly (MCA, AD 800–1300). Similar trends in flood frequency were observed in the European Alps (e.g. Glur et al., 2013; Swierczynski et al., 2013; Wirth et al., 2013; Wilhelm et al., 2013) and in the north-western Mediterranean area (Moreno et al., 2008; Arnaud-Fassetta

et al., 2010; Wilhelm et al., 2012a; Benito et al., 2015; Wilhelm et al., 2016a). An increase in flood intensity during the LIA was also observed in Lake Allos, a site located 100 km south and also strongly influenced by the Mediterranean climate (Wilhelm et al., 2012a).

Over the whole studied period, the Savine record show similarities with the stacked flood-frequency records of the southern Alps, also strongly influenced by the Mediterranean climate, from Wirth et al. (2013), (Figure 8C). This record shows a relatively low flood activity during the early Holocene followed by a sharp increase of flood frequency at 4.2 kyr BP that lasts over the entire Late Holocene. This main change at 4.2 kyr BP is also recorded in Lake Ledro (Vannière et al., 2013) and Lake Savine, but here dated at 3.9 kyr BP. This time lag between records may be linked to i) the respective age-model uncertainties (3.8-4.02 kyrs BP for Savine) or ii) to the northernmost position of Lake Savine, that might explain a latter impact latter of Mediterranean climate change. Vannière et al., (2013) and Magny et al., (2013) attributed this transition to a nonlinear climate response to the orbitally driven gradual decrease in summer insolation at 60°N (Figure 8E, Berger and Loutre, 1991). This would control the millennial trend toward wetter conditions during the late Holocene (Mayewski et al., 2004). In the Savine palaoflood record, the flood frequency also shows a generally high level after 4.2 kyr BP. However, periods of increased flood frequency are still observable at the millennial timescale at 3.9-2.35, 2-1.5, 1.15-1.05 and 0.65-0.05 kyr BP. These periods are synchronous with the stacked S-Alps records (grey bands Figure 8A, C) and mainly corresponds to Holocene cold events (Bond et al., 2001; Mayewski et al., 2004; Wanner et al., 2011). These periods are known to have produced a stronger meridional temperature gradient and thus a southward position of the westerlies with higher storm activity in the Western Mediterranean area (Sabatier et al., 2012). During this same period, at the centennial timescale, this synchronism is still remarkable (dotted line in Figure 8A, C) supporting the hypothesis that dominated precipitation pattern is the same in these two areas, as shown from historical events reanalysis. Before 4.2 kyr BP Savine flood frequency presents a main increase between 5.6 and 4.85 kyr BP that is not recorded in the Southern Alps, this may suggest that these records are decoupled before 4.2 kyr BP. The Lake Anterne (Northern French Alps) paleoflood record also presents an increase in flood frequency between 5.6-4.6 kyr BP (Figure 6B, G) (Giguet-Covex et al., 2011). This increase in flood frequency is also observed in other paleohydrological record as in the lake du Bourget (centered aroud 5.5 kyr BP, Arnaud et al., 2012) and in Centrale Europe (between 5.5 and 5 kyr BP, Czymzik et al., 2016). This increase is also shown in the stacked palaeoflood records produced in the northern Alps by Wirth et al., (2013). Thus, the flood frequency at Savine seems to be in phase with Northern Alps paleoflood reconstruction before 4.2 kyr BP and with Southern paleoflood reconstruction after this period. Over the last millennium, the Northern French Alps is mostly dominated by localized summer convective precipitation events (Wilhelm et al., 2013). As the study site could also record summer thunderstorms, we propose that before the 4.2 kyr BP climate transition, this atmospheric event could be the dominant precipitation pattern.

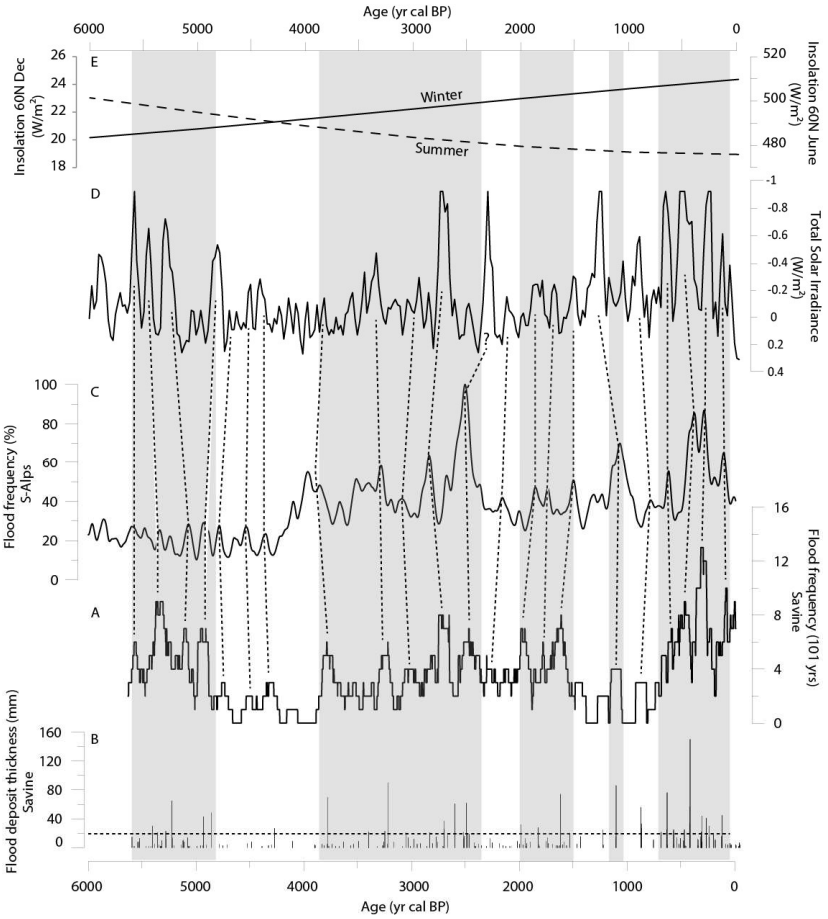

Figure 8: Comparison of (A) reconstructed Savine flood frequency (101 yrs running average) and (B) intensity (thickness of flood deposits) with (C) stacked S-Alps flood frequency (100-year low-pass filtered) Wirth et al., (2013), (D) Total Solar Irradiance (TSI) Steinhilber et al., (2012) and (E) June and Dec. insolation at 60°N (Berger and Loutre, 1991). Vertical gray areas mark high frequency and intensity flood periods record in Savine on multi-centennial timescale. Dotted line try to correlate, on secular timescale, period of high flood frequency record in Savine with both high S-Alps flood frequency and of low solar activity period, all these correlation are in the age model uncertainties.

The Savine flood frequency presents 22 short term increases (dotted lines in Figure 8) mostly associated with high intensity. Each of these sharp increase seems synchronous to well-marked increases in TSI (Figure 8A, D; Steinhilber et al., 2012), suggesting increasing flood frequency

and intensity during periods of solar minima. Over the last 1400 yrs BP, Wilhelm et al., (2012a) show that major multi-centennial changes in extreme precipitation patterns (frequency and intensity) in the Southern Alps occur during cooling phases, such as the LIA and are associated to solar activity. Similarly, Wirth et al., (2013) suggested a strong solar influence on the Mediterranean precipitation regime because they observed a synchronous variability between low TSI cycles the high S-Alpine flood frequency. In the same way, in Central Europe (southern Germany), Czymzik et al., (2016) found that flood frequency is higher when solar activity is reduced. Hence, large changes in solar radiation (grand solar minima) indirectly affect climate by inducing atmospheric changes in a large European Atlantic sector (Martin-Puertas, et al., 2012) resulting also in higher flood frequency but also intensity in the Savine area. Several studies show that periods of a long-term reduction in solar radiation induce a North Atlantic storm tracks shift further south with a maximum over the Mediterranean Sea, carrying more humid air masses to Central and Southern Europe (e.g. Raible et al., 2007; Martin-Puertas, et al., 2012). In this scenario, the part of the Alps influenced by the proximity of the Mediterranean Sea climate likely experienced an increase in flood frequency and intensity because of an increase in moisture advection from the North Atlantic.

Finally, our results suggest that the occurrence and the intensity of extreme precipitation events triggering mountain-river floods may be influenced by both lower temperature on millennial timescale and solar forcing through change in atmospheric pattern on a centennial scale. Even if, we cannot rule out future changes in TSI and its effect on flood occurrence, the current global change with higher temperatures lead to less extreme precipitation events in this area. But, higher temperatures lead also to more efficient convection (Beniston et al., 2007; Giorgi et al., 2016), thereby producing very heavy local rainfall events and, in turn, high intensity flood events. As this type of precipitation pattern account for a small a part of historical record events, we can not exclude with an unprecedented warming a future increase of this type of event.

6. Conclusion

The high-resolution sedimentological and geochemical analyses of the Lake Savine sediment sequence allowed to identify 220 turbidites over the last 6000 years. Twenty of the 220 turbidites can be differentiated by grain size parameters and geochemical features (low Mn contents) and are most probably results from mass movements. These events are disturbed in 5 clusters over this period and are possibly related to earthquakes in regard to their correlation to historic and paleo earthquake in this region. For the other 200 turbidites we found a strong relationship between deposit thickness and coarse fraction content (Q90max), suggesting that these turbidites were produced by floods and that deposit thickness can be used as a high resolution proxy for palaeoflood intensity. The local human activity is reconstructed through ancient DNA and reveals that ovin and bovin are present in the catchment only during a restricted period between 2.05 and 1.75 kyr BP. But no changes is observed in the grainsize versus deposit thickness pattern during this period suggesting a minor influence of human activity on erosion processes and, thereby, on the reconstructed flood chronicle.

Weather reanalysis of historical floods record in the Savine sequence show that floods represent past variability of mainly mesoscale events called “East-return” events (75%) and at lower extend local summer convective events (i.e. thunderstorms). At multi-centennial timescale the Savine flood chronicle shows five periods of high flood frequency and intensity between 5.6-4.85, 3.9-2.35, 2-1.5, 1.15-1.05 and 0.65-0.05 kyr BP. These periods correspond mainly to Holocene cold events and are in good agreement with previous reconstructed flood frequency reconstructed from northern Alpine region between 6 to 4 kyr BP and from southern Alpine region between 4 kyr BP and today. The paleohydrological transition at 4 kyr BP may result from an abrupt change from Atlantic to Mediterranean climatic influences on the flood activity in this Alpine area and could correspond to the observed transition in Mediterranean area during this period. At centennial timescale increase in flood frequency and intensity at Savine occurs during periods of solar minima. These long-term reduction in solar radiation probably affect indirectly the climate in a large European Atlantic sector through atmospheric changes with a southward shift in the North Atlantic storm tracks and a maximum over the Mediterranean Sea. During these periods more humid air masses are transported to the Alpine region influenced by the proximity of the Mediterranean Sea and induced an increase in flood frequency and intensity.

Acknowledgments

This research was performed by Hannibal Project financed by the DIPEE (Dispositifs de Partenariat en Ecologie et Environnement) Chambéry Grenoble of the CNRS INEE. We thank the town of Bramand for the coring authorization. The authors thank CLIMCORE Continent for coring facilities. 14C analyses were acquired, thanks to the CNRS-INSU ARTEMIS national radiocarbon AMS measurement program at Laboratoire de Mesure 14C (LMC14) in the CEA Institute at Saclay (French Atomic Energy Commission). The authors thank the Laboratoire Souterrain de Modane (LSM) facilities for the gamma spectrometry measurements and Environnement, Dynamique et Territoires de Montagne for the X-ray fluorescence analyses.

References:

- Alric, B., Jenny, J.P., Berthon, V., Arnaud, F.,Pignol, C., Reyss, J.L., Sabatier, P., Perga, M.E. (2013). Local forcings affect lake zooplankton vulnerability and response to climate warming. Ecology, 94, 2767–2780.
- Appleby PG (1991) 241Am dating of lake sediments. Hydrobiologia 214:35–42.
- Arnaud, F., Lignier, V., Revel, M., Desmet, M., Beck, C., Pourchet, M., Charlet, F., Trentesaux, A., Tribovillard, N., 2002. Flood and earthquake disturbance of 210Pb geochronology (Lake Anterne, NW Alps). Terra Nova 14, 225–232.
- Arnaud, F., Poulenard, J., Giguet-Covex, C.,Wilhelm, B., Révillon, S., Jenny, J.P., Enters, D., Bajard, M., Fouinat, L., Doyen, E., Simonneau, A., Chapron, E., Vannière, B., Sabatier, P.. Erosion under climate and human pressures: an alpine lake sediment perspective. Submitted to Quaternary Science Review.

- Arnaud-Fassetta, G. and Fort, M., (2004). Respective parts of hydroclimatic and anthropic factors in the recent eveolution (1956–2000) of the active channel of the Upper Guil, Queyras, Southern French Alps, Méditerranée, 102, 143–156.
- Arnaud-Fassetta, G., Carcaud, N., Castanet, C., and Salvador, P.G. (2010). Fluviatile palaeoenvironments in archaeological context: geographical position, methodological approach and global change hydrological risk issues, Quatern. Int., 216, 93–117.
- Bajard, M., Sabatier, P., David, F., Develle, A.L., Reyss, J.L., Fanget, B., Malet, E., Arnaud, D., Augustin, L., Crouzet, C., Poulenard, J., Arnaud, F. (2016). Erosion record in Lake La Thuile sediments evidences montane landscape dynamics through the Holocene. Holocene, 26(3) 350-364.
- Beck, C., 2009. Late Quaternary lacustrine paleo-seismic archives in north-western Alps: examples of earthquake-origin assessment of sedimentary disturbances. Earth Sci. Rev. 96, 327–344.
- Beniston, M. and Stephenson, D. B. (2004). Extreme climatic events and their evolution under changing climatic conditions, Glob. Planet. Change, 44, 1–9.
- Beniston M, Stephenson DB, Christensen OB, Christopher A. T. Ferro, Frei, C., Goyette, S., Halsnaes, K., Holt, T., Jylhä, K., Koffi, B., Palutikof, J., Schöll, R., Semmler, T., Woth, K., T. (2007). Future extreme events in European climate: an exploration of regional climate model projections. Climatic Change 81: 71–95.
- Berger, A. and Loutre, M. F. (1991). Insolation values for the climate of the last 10 million years, Quaternary Sci. Rev., 10, 297–317.
- Benito, G., Macklin, M. G., Zielhofer, C., Jones A., and Machado, M. J. (2015). Holocene flooding and climate change in the Mediterranean, Catena, 130, 13–33.
- Binladen, J., Gilbert, M.T.P., Bollback, J.P., Panitz, F., Bendixen, C., Nielsen, R., Willerslev, E., 2007. The Use of Coded PCR Primers Enables High-Throughput Sequencing of Multiple Homolog Amplification Products by 454 Parallel Sequencing. PLoS ONE 2.
- Blaauw M. (2010). Methods and code for 'classical' age-modelling of radiocarbon sequences. Quaternary Geochronology, 5(5), 512–518.
- Bøe, A.-G., Dahl, S.O., Lie, Ø., Nesje, A., 2006. Holocene river floods in the upper Glomma catchment, southern Norway: a high-resolution multiproxy record from lacustrine sediments. The Holocene 16, 445–455.
- Bond, G., Kromer, B., Beer, J., Muscheler, R., Evans, M.N., Showers, W., Hoffmann, S., Lotti-Bond, R., Hajdas, I., Bonani, G., 2001. Persistent solar influence on North Atlantic climate during the Holocene. Science 294, 2130–2136.
- Boschi, E., Guidoboni, E., Ferrari, G., Mariotti, D., Valensise, G. and Gasperini, P. ed. 2000. 'Catalogue of Strong Italian Earthquakes From 461 B.C. to 1997. Introductory Texts and CD-ROM' Annali di Geofisica 43, 4.
- Boyer, F., Mercier, C., Bonin, A., Le Bras, Y., Taberlet, P., Coissac, E., 2016. obitools: a unix-inspired software package for DNA metabarcoding. Molecular Ecology Resources 16, 176-182.
- Calvert SE and Pedersen TF (1993) Geochemistry of recent oxic and anoxic marine sediments: Implications for the geological record. Marine Geology 113(1): 67–88.

- CEA (2007). Reducing the social and economic impact of climate change and natural catastrophes: insurance solutions and public private partnerships. Insurers of Europe, Brussels.
- Chapron, E., Beck, C., Pourchet, M., Deconinck, J.-F., 1999. 1822 AD earthquake-triggered homogenite in Lake Le Bourget (NW Alps). Terra Nova 11, 86–92.
- Chapron E., Simonneau A., Ledoux G., Arnaud F., Lajeunesse P., Albéric P. (2016). French alpine foreland Holocene paleoseismicity revealed by coeval mass wasting deposits in glacial lakes. Springer International Publishing Switzerland 2016, G. Lamarche et al. (eds.), Submarine Mass Movements and their Consequences, Advances in Natural and Technological Hazards Research, 41, Chapter 34 pp 341- 349.
- Compo GP, Whitaker JS, Sardeshmukh PD, Matsui N, Allan RJ, Yin X, Gleason BE, Vose RS, Rutledge G, Bessemoulin P, Bronnimann S, Brunet M, Crouthamel RI, Grant AN, Groisman PY, Jones PD, Kruk M, Kruger AC, Marshall GJ, Maugeri M, Mok HY, Nordli O, Ross TF, Trigo RM, Wang XL, Woodruff SD, Worley SJ. (2011). The Twentieth Century Reanalysis Project. Q. J. R. Meteorol. Soc., 137, 1–28.
- Corella, J. P., Benito, G., Rodriguez-Lloveras, X., Brauer, A., and Valero-Garcès, B. (2014). Annually-resolved lake record of extreme hydro-meteorological events since AD 1347 in NE Iberian Peninsula, Quaternary Sci. Rev., 93, 77–90.
- Czymzik, M., Muscheler, R., Brauer, A. (2016). Solar modulation of flood frequency in central Europe during spring and summer on interannual to multi-centennial timescales. Climate of the Past, 12, 799–805.
- Doyen, E., Vanniere, B., Berger, J.-F., Arnaud, F., Tachikawa, K., Bard, E., 2013. Land-use changes and environmental dynamics in the upper Rhone valley since Neolithic times inferred from sediments in Lac Moras. The Holocene 23, 961–973. doi:10.1177/0959683612475142
- Durant, Y., Laternser, M., Giraud, G., Etchevers, P., Lesaffre, B., Merindol, L. (2009). Reanalysis of 44 Yr of Climate in the French Alps (1958–2002): Methodology, Model Validation, Climatology, and Trends for Air Temperature and Precipitation, J. Appl. Meteorol. Climatol., 48, 429–449.
- Elbaz-Poulichet, F., Sabatier, P., Dezileau, L., Freydier, R. (2014). Sedimentary record of V, U, Mo and Mn in the Pierre-Blanche lagoon (Southern France) - Evidence for a major anoxia event during the Roman period. Holocene, 24(10), 1384–1392.
- Etienne, D., Wilhelm, B., Sabatier, P., Reyss, J.-L., Arnaud, F., 2013. Influence of sample location and livestock numbers on Sporormiella concentrations and accumulation rates in surface sediments of Lake Allos, French Alps. Journal of Paleolimnology 49, 117-127.
- Ficetola GF, Taberlet P, Coissac E (2016) How to limit false positives in environmental DNA and metabarcoding? Mol Ecol Resour 16:604-607.
- Ficetola, G.F., Pansu, J., Bonin, A., Coissac, E., Giguet-Covex, C., De Barba, M., Gielly, L., Martins Lopes, C., Boyer, F., Pompanon, F., Rayé, J., Taberlet, P., 2015. Replication levels, false presences, and the estimation of presence / absence from eDNA metabarcoding data. Molecular Ecology Resources 15, 543–556.
- Ficetola, G.F., Coissac, E., Zundel, S., Riaz, T., Shehzad, W., Bessière, J., Taberlet, P., Pompanon, F., 2010. An In silico approach for the evaluation of DNA barcodes. BMC Genomics 11, 434.

- Fouinat, L., Sabatier, P., Poulenard, P., Etienne, D., Crouzet, C., Develle, A.L., Doyen, E., Malet, E., Reyss, J.L., Bonnet, R., Arnaud, F. 1700 years of interaction between glacial activity and flood frequency in proglacial Lake Muzelle (western French Alps). Accepted to Quaternary Research.
- Garavaglia F, J. Gailhard, E. Paquet, M. Lang, R. Garcon, and P. Bernardara. (2010). Introducing a rainfall compound distribution model based on weather patterns sub-sampling. Hydrol. Earth Syst. Sci. 14, 951-964.
- Gaume, E., Bain, V., Bernardara, P., Newinger, O., Barbuc, M., Bateman, A., Blaškovicová, L., Blöschl, G., Borga, M., Dumitrescu, A., Daliakopoulos, I., Garcia, J., Irimescu, A.,Kohnova, S., Koutroulis, A., Marchi, L., Matreata, S., Medina, V., Preciso, E., Sempere-Torres, D., Stancalie, G., Szolgay, J., Tsanis, I., Velasco, D., Viglione, A., 2009. A compilation of data on European flash floods. Journal of Hydrology 367, 70–78.
- Giguet-Covex, C., Arnaud, F., Poulenard, J., Disnar, J.-R., Delhon, C., Francus, P., David, F., Enters, D., Rey, P.-J., Delannoy, J.-J., 2011. Changes in erosion patterns during the Holocene in a currently treeless subalpine catchment inferred from lake sediment geochemistry (Lake Anterne, 2063 m a.s.l., NW French Alps): The role of climate and human activities. The Holocene 21, 651–665. doi:10.1177/0959683610391320
- Giguet-Covex, C., Arnaud, F., Enters, D., Poulenard, J., Millet, L., Francus, P., David, F., Rey, P.-J., Wilhelm, B., Delannoy, J.-J., 2012. Frequency and intensity of high-altitude floods over the last 3.5ka in northwestern French Alps (Lake Anterne). Quat. Res. 77, 12–22. doi:10.1016/j.yqres.2011.11.003
- Giguet-Covex, C., Pansu, J., Arnaud, F., Rey, P.-J., Griggo, C., Gielly, L., Domaizon, I., Coissac, E., David, F., Choler, P., 2014. Long livestock farming history and human landscape shaping revealed by lake sediment DNA. Nature communications 5
- Giorgi, F., Torma, C., Coppola, E., Ban, N., Schär, C., Somot, S. (2016). Enhanced summer convective rainfall at Alpine high elevations in response to climate warming. Nature Geoscience, DOI: 10.1038/NGEO2761.
- Glur, L.,Wirth, S. B., Buntgen, U., Gilli, A., Haug, G. H., Schär, C., Beer, J., and Anselmetti, F. S. (2013). Frequent floods in the European Alps coincide with cooler periods of the past 2500 years, Sci., Rep., 3, 2770, doi:10.1038/srep02770.
- Golberg E (1963) Geochronology with 210Pb. Radioactive Dating (International Atomic Energy Agency, Vienna), pp 121–131.
- Gottardi, F., Obled, C., Gailhard, J., Paquet, E. (2010). Statistical reanalysis of precipitation fields based on ground network data and weather patterns: Application over French mountains, J. Hydrol., 432/433, 154–167.
- Guédron, S., Amouroux, D., Sabatier, P., Desplanque, C., Develle, A.L., Barre, J., Feng, C., Guiter, F., Arnaud, F., Reyss, J.L., Charlet, L. (2016). A 150-year record of industrial and urban development in French Alps combining Hg accumulation rates and isotope composition in sediment archives from Lake Luitel. Chemical Geology, 431, 10-19.
- Hodder, K.R., Gilbert, R., Desloges, J.R., 2007. Glaciolacustrine varved sediment as an alpine hydroclimatic proxy. J. Paleolimnol. 38, 365–394.
- IPCC 2013: The Physical Science Basis, Contribution of Working Group I to the Fifth Assessment Report of the Intergovernmental Panel on Climate Change, edited by: Stocker, T. F., Qin, D., Plattner, G.-K., Tignor, M., Allen, S. K., Boschung, J., Nauels, A., Xia, Y., Bex,

V., and Midgley, P. M., Cambridge University Press, Cambridge, United Kingdom and New York, NY, USA.
- Jenny, J.P., Arnaud, F., Dorioz, J.M., Giguet Covex, C., Frossard, V., Sabatier, P., Millet, L., Reyss, J.L., Tachikawa, K., Bard, E., Pignol, C., Perga, M.E. (2013). A spatiotemporal sediment investigation highlights the dynamics of hypolimnetic hypoxia in large perialpine Lake Bourget over the last 150 years. Limnology and Oceanography, 58, 1395-1408.
- Kéry M (2010) Introduction to WinBUGS for ecologists. Academic Press, Burlington, MA.
- Koppes, M.N., Hallet, B., 2002. Influence of rapid glacial retreat on the rate of erosion by tidewater glaciers. Geology 30, 47–50.
- Lambert, J., and A. Levret-Albaret (1996), Mille ans de Séismes en France. Catalogues d'Épicentres, Paramètres et Références, Ouest-Editions ed., 78 pp., Presses Académiques, Nantes.
- Lionello, P., Abrantes, F., Congedi, L., Dulac, F., Gacic, M., Gomis, D., Goodess, C., Hoff, H., Kutiel, H., Luterbacher, J., Planton, S., Reale, M., Schröder, K., Struglia, M. V., Toreti, A., Tsimplis, M., Ulbrich, U., and Xoplaki, E., (2012). Introduction: Mediterranean Climate: Background Information, edited by: Lionello, P., The Climate of the Mediterranean Region, From the Past to the Future, Amsterdam: Elsevier (Netherlands), XXXV–lXXX, ISBN:9780124160422.
- Lahoz-Monfort JJ, Guillera-Arroita G, Tingley R (2016) Statistical approaches to account for false positive errors in environmental DNA samples. Mol Ecol Resour 16:673–685.
- Magny, M., Combourieu Nebout, N., de Beaulieu, J. L., Bout-Roumazeilles, V., Colombaroli, D., Desprat, S., Francke, A., Joannin, S., Peyron, O., Revel, M., Sadori, L., Siani, G., Sicre, M.A., Samartin, S., Simonneau, A., Tinner, W., Vannière, B., Wagner, B., Zanchetta, G., Anselmetti, F., Brugiapaglia, E., Chapron, E., Debret, M., Desmet, M., Didier, J., Essallami, L., Galop, D., Gilli, A., Haas, J. N., Kallel, N., Millet, L., Stock, A., Turon, J.L., and Wirth, S. (2013). North–south palaeohydrological contrasts in the central Mediterranean during the Holocene: tentative synthesis and working hypotheses, Clim. Past, 9, 1901–1967.
- Martin-Puertas, C., Matthes, K., Brauer, A., Muscheler, R., Hansen, F., Petrick, C., Aldahan, A., Possnert, G., van Geel, B. (2012). Regional atmospheric circulation shifts induced by a grand solar minimum. Nat. Geosci. 5, 397–401.
- Mayewski, P.A., Rohling, E.E., Stager, J.C., Karlen, W., Maasch, K.A., Meeker, L.D., Meyerson, E.A., Gasse, F., van Kreveld, S., Holmgren, K., Lee-Thorp, J., Rosqvist, G., Rack, F., Staubwasser, M., Schneider, R.R., Steig, E.J., 2004. Holocene climate variability. Quaternary Research 62, 243–255.
- Molinaroli, E., Guerzoni, S., De Falco, G., Sarretta, A., Cucco, A., Como, S., 2009. Relationships between hydrodynamic parameters and grain size in two contrasting transitional environments: the lagoons of Venice and Cabras, Italy. Sedimentary Geology 219, 196–207.
- Moreno, A., Valero-Garces, B. L., Gonzalez-Samperiz, P., and Rico, M. (2008). Flood response to rainfall variability during the last 2000 years inferred from the Taravilla Lake record (Central Iberian Range, Spain), J. Palaeolimnol., 40, 943–961.
- Mulder, T. and Cochonat, P.: Classification of offshore mass movements, J. Sediment. Res., 66, 43–57, 1996.

- Noren, A. J., Bierman, P. R., Steig, E. J., Lini, A., and Southon, J. (2002). Millennial-scale storminess variability in the northeastern United States during the Holocene epoch, Nature, 419, 821–824.
- Pansu, J., Giguet-Covex, C., Ficetola, G.F., Gielly, L., Boyer, F., Zinger, L., Arnaud, F., Poulenard, J., Taberlet, P., Choler, P., 2015. Reconstructing long-term human impacts on plant communities: an ecological approach based on lake sediment DNA. Molecular Ecology 24, 1485–1498.
- Parris, A.S., Bierman, P.R., Noren, A.J., Prins, M.A., Lini, A., 2010. Holocene paleostorms identified by particle size signatures in lake sediments from the northeastern United States. Journal of Paleolimnology 43 (1), 29–49.
- Pedersen TF and Price NB (1982). The geochemistry of manganese carbonate in Panama Basin sediments. Geochimica et Cosmochimica Acta 46(1): 59–68.
- Petersen, J., Wilhelm, B., Revel, M., Rolland, Y., Crouzet, C., Arnaud, F., Magand, O., Chaumillon, E., 2014. Sediment archive of Lake Vens (SW European Alps, France) as a record of large magnitude earthquakes. J. of Paleolimnol. 51, 343–355.
- R Development Core Team (2011) R: A Language and Environment for Statistical Computing. Vienna: R Foundation for Statistical Computing. Available at:
- Raible, C. C., Yoshimori, M., Stocker, T. F., and Casty, C. (2007). Extreme midlatitude cyclones and their implications for precipitation and wind speed extremes in simulations of the Maunder Minimum versus present day conditions, Clim. Dynam., 28, 409–423.
- Ratto, S., Bonetto, F., and Comoglio, C. (2003). The October 2000 flooding in Valle d'Aosta (Italy): Event description and land planning measures for the risk mitigation. International Journal of River Basin Management, 1(2), 105-116.
- Ratzov, G., Cattaneo, A., Babonneau, N., Déverchère, J., Yelles, K., Bracene, R., Courboulex, F. (2015). Holocene turbidites record earthquake supercycles at a slow-rate plate boundary. Geology v. 43; no. 4; p. 331–334.
- Reimer, P.J., Bard, E., Bayliss, A., Beck, J.W., Blackwell, P.G., Bronk Ramsey, C., Buck, C.E., Cheng, H., Edwards, R.L., Friedrich, M., others, (2013). IntCal13 and Marine13 radiocarbon age calibration curves 0-50,000 years cal BP.
- Reyss J.L., Schimdt S., Legeleux F., Bonte P. (1995). Large low background well type detectors for measurements of environmental radioactivity. Nucl Instrum Methods 357: 391–397.
- Richter, T.O., Van der Gaast, S.J., Koster, B., Vaars, A.J., Gieles, R., De Stigter, H.C., De Haas, H., VanWeering, T.C.E., 2006. The Avaatech XRF Core Scanner: technical description and applications to NE Atlantic sediments. In: Rothwell, R.G. (Ed.), NewTechniques in Sediment Core Analysis. : Special Publications. Geological Society, London, pp. 39–50.
- Rimbu, N., Czymzik, M., Ionita, M., Lohmann, G., Brauer, A. (2016). Atmospheric circulation patterns associated with the variability of River Ammer floods: evidence from observed and proxy data. Clim. Past, 12, 377–385.
- Sabatier P., Dezileau L., Briqueu L., Colin C., Siani G. (2010). Clay minerals and geochemistry record from Northwestern Mediterranean coastal lagoon sequence: Implications for paleostorm reconstruction. Sed Geol 228:205–217.

- Sabatier, P., Dezileau, L., Colin, C., M., Briqueu, L., Martinez, P., Siani, G., Bouchette, F., Raynal, O. and Von Grafenstein, U. (2012). 7000 years of paleostorm activity in the NW Mediterranean Sea in response to Holocene climate events. Quarternary Research 77, 1-11.
- Sabatier, P., Poulenard, J., Fanget, B., Reyss, J.L., Develle, A.L., Wilhelm, B., Ployon, E., Pignol C., Naffrechoux, E., Dorioz, J.M., Montuelle, B., Arnaud, F. (2014). Secular interplays between pesticides and erosion in vineyards. PNAS, 111(44), 15647–15652.
- Simonneau, A., Doyen, E., Chapron, E., Millet, L., Vannière, B., Di Giovanni, C., Bossard, N., Tachikawa, K., Bard, E., Albéric, P., Desmet, M., Roux, G., Lajeunesse, P., Berger, J.F., Arnaud, F., 2013b. Holocene land-use evolution and associated soil erosion in the French Prealps inferred from Lake Paladru sediments and archaeological evidences. J. Archaeol. Sci. 40, 1636–1645. doi:10.1016/j.jas.2012.12.002
- Scotti, O., D. Baumont, G. Quenet, and A. Levret (2004), The French macroseismic database SISFRANCE: Objectives, results and perspectives, Ann. Geophys., 47(2), 571–581.
- Steinhilber, F., Abreu, J. A., Beer, J., Brunner, I., Christ l, M., Fischer, H., Heikkilä, U., Kubik, P. W., Mann, M., McCracken, K., Miller, H., Miyahara, H., Oerter, H., and Wilhelms, F. (2012). 9,400 years of cosmic radiation and solar activity from ice cores and tree rings. PNAS, 109, 5967.
- Sturm, M., Matter, A., (1978). Turbidites and varves in Lake Brienz (Switzerland): deposition of clastic detritus by density currents. Special Publications of International Association of Sedimentologists 2, 147–168.
- Su YS, Yajima M (2015) R2jags: Using R to Run 'JAGS'. R package version 0.5-7. www.r-project.org
- Swierczynski, T., Lauterbach, S., Dulski, P., Delgado, J., Merz, B., Brauer, A. (2013). Mid- to late Holocene flood frequency changes in the northeastern Alps as recorded in varved sediments of Lake Mondsee (Upper Austria), Quaternary Sci. Rev., 80, 78–90.
- Taberlet, P., Prud'homme, S.M., Campione, E., Roy, J., Miquel, C., Shehzad, W., Gielly, L., Rioux, D., Choler, P., Clement, J.C., Melodelima, C., Pompanon, F., Coissac, E., 2012. Soil sampling and isolation of extracellular DNA from large amount of starting material suitable for metabarcoding studies. Molecular Ecology 21, 1816-1820.
- Valentini, A., Miquel, C., Nawaz, N., Bellemain, E., Coissac, E., Pompanon, F., Gielly, L., Cruaud, C., Nascetti, G., Wincker, P., Swenson, J., Taberlet, P., 2009. New perspectives in diet analysis based on DNA barcoding and parallel pyrosequencing: the trnL approach. Molecular Ecology Resources 9, 51-60.
- Vannière, B., Magny, M., Joannin, S., Simonneau, A., Wirth, S.B., Hamann, Y., Chapron, E., Gilli, A., Desmet, M., Anselmetti, F.S., (2013). Orbital changes, variation in solar activity and increased anthropogenic activities: controls on the Holocene flood frequency in the Lake Ledro area, Northern Italy. Clim. Past 9, 1193-1209.
- Wanner, H., Solomina, O., Grosjean, M., Ritz, S.P., Jetel, M., 2011. Structure and origin of Holocene cold events. Quat. Sci. Rev. 30, 3109-3123.
- Westra, S., L. V. Alexander, and F. W. Zwiers (2013), Global increasing trends in annual maximum daily precipitation, J. Clim., 26, 3904-3918.
- Whitaker JS, Hamill TM. 2002. Ensemble data assimilation without perturbed observations. Mon. Weather Rev., 130, 1913–1924.

- Wilhelm, B., Arnaud, F., Sabatier, P., Crouzet, C., Brisset, E., Chaumillon, E., Disnar, J.R., Guiter, F., Malet, E., Reyss, J.L., Tachikawa, K., Bard, E. and Delannoy, J.J. (2012a). 1.4 kyrs of flash flood events in the Southern European Alps : implications for extreme precipitation patterns and forcing over the north western Mediterranean area. Quaternary Research, 78, 1-12.
- Wilhelm, B., Arnaud, F., Enters, D., Allignol, F., Legaz, A., Magand, O., Revillon, S., Giguet-Covex, C., Malet, E., (2012b). Does global warming favour the occurrence of extreme floods in European Alps? First evidences from a NW Alps proglacial lake sediment record, Climatic Change. DOI: 10.1007/s10584-011-0376-2.
- Wilhelm, B., Vogel, H., Crouzet, C., Etienne, D., Anselmetti, F.S. (2016a). Frequency and intensity of palaeofloods at the interface of Atlantic and Mediterranean climate domains. Clim. Past, 12, 299–316.
- Wilhelm, B., Nomade, J., Crouzet, C., Litty, C., Sabatier, P., Belle, S., Rolland, Y., Revel, M., Courboulex, F., Arnaud, F., Anselmetti, F.S. (2016b). Quantified sensitivity of lake sediments to record historic earthquakes : Implications for paleoseismology. Journal of Geophysical Research, 121(1), 2–16.
- Wirth S. B., Glur, L., Gilli, A., and Anselmetti, F. S.: Holocene flood frequency across the Central Alps – solar forcing and evidence for variations in North Atlantic atmospheric circulation, Quaternary Sci. Rev., 80, 112–128, 2013.

Supplementary Information:

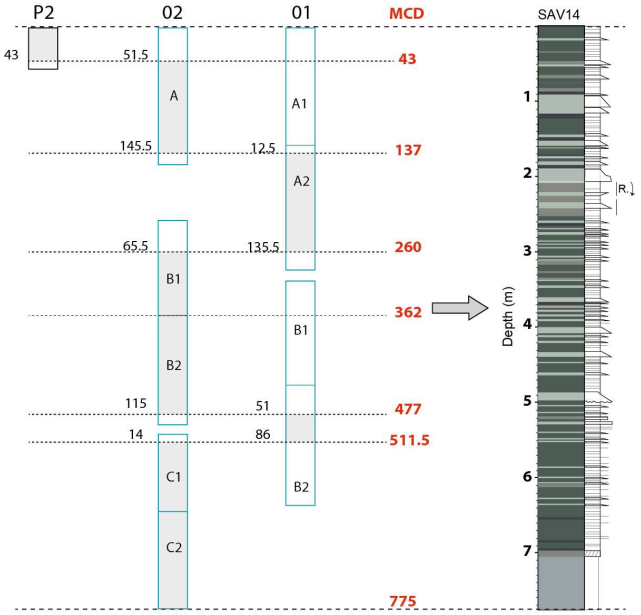

Figure SI1: Savine composite sediment sequence built from noticeable layers (depth of these layers indicated in dark form the top of section and in red from the lake sediment interface) from the overlapping sections of all cores. The utile section to build the master core is indicated in grey.

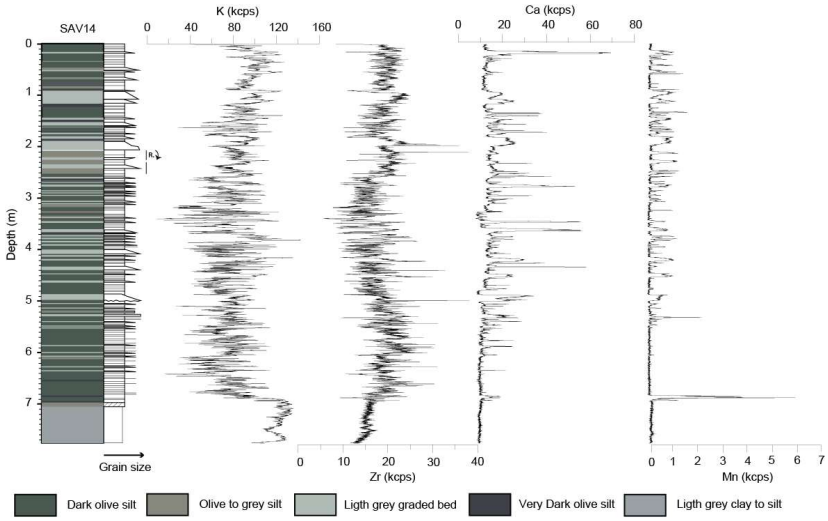

Figure SI2: Lithological description of the Savine master core with geochemical variations for selected elements (K, Zr, Ca, Mn) expressed in kcps.

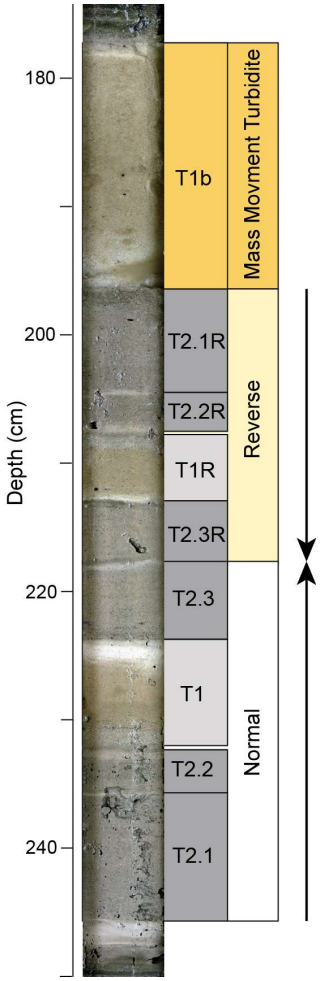

Figure SI3: Photography and sedimentology interpretation of the remarkable 22 cm reversal sequence observed between 196 and 218 cm of the mastercore overlapped by a 17cm turbidite (T1b). T2.X and T1 correspond to the 2 main deposits described in the result part of the manuscript, X correspond to the chronology of the deposit (1 older than 3). R suffixes denote the reversal position of previous described deposit.

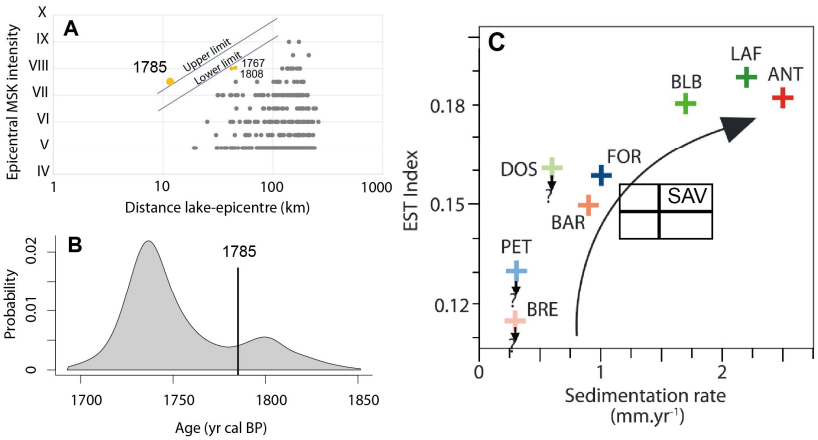

Figure SI4: (A) Diagram "distance of earthquakes to the lake versus epicentral MSK intensity", grey dots indicate all historic earthquakes closer than 250 km to the Lake Savine with epicentral MSK intensities ≥IV. Orange dots with dates correspond to historic earthquakes correlated to the most recent T2 deposit. The limits of sensitivity (continuous lines) are placed to delimit the recorded from non-recorded earthquakes, with upper and lower limits, the slope is define by Wilhelm et al., (2016b). (B) Probability distribution frequencies of the first T2 deposit ages and possible correlations to the 1785 historical earthquake (vertical line). (C) The Lake Savine sedimentation rate and ESTI index (black rectangle, link to the uncertainties of ESTI calculation and the variation of the sedimentation rate) plotted with previous results from Wilhelm et al. (2016b).